AIAA JOURNAL
Vol. 49, No. 5, May 2011

Validity of Amiet's Model for Propeller Trailing-Edge Noise

Vincent P. Blandeau* and Phillip F. Joseph†
University of Southampton, Southampton, England SO45 4NT, United Kingdom

DOI: 10.2514/1.J050765

This paper presents a fundamental investigation into the validity of the classical model by Amiet for predicting the broadband trailing-edge noise due to rotating blades. This approximate model is compared analytically against a model in which the effects of rotation are treated exactly. Low- and high-frequency limits are identified, within which Amiet's model is in excellent agreement with the exact solution. Estimates of the error of Amiet's model outside of these limits are also provided. The method is illustrated by application to an open propeller, a model cooling fan, and a wind turbine. The use of Amiet's model for treating the effects of rotation can provide substantial reductions in computation time when the unsteady blade response is computed from computationally demanding methods, such as computational fluid dynamics.

Nomenclature

B	=	blade number
c	=	airfoil chord
C_f	=	friction coefficient
c_0	=	speed of sound
D_k	=	directivity function of exact model
D_ϕ	=	directivity function of Amiet's model
$d\mathbf{F}$	=	elemental force applied by blade on fluid
f_{high}	=	high-frequency limit of validity of Amiet's model
f_{low}	=	low-frequency limit of validity of Amiet's model
f_{shaft}	=	shaft frequency, $\Omega/2\pi$
k	=	acoustic azimuthal mode order
k_r, k_X	=	spanwise and chordwise wave numbers of turbulence
k_0	=	acoustic wave number, ω/c_0
$\mathcal{L}$	=	aeroacoustic coupling term
l_r	=	spanwise correlation length
M_x	=	flight Mach number
M_ϕ	=	rotation Mach number
$\bar{r}$	=	radial location of midspan of blade strip
$S_{pp,\text{Amiet}}$	=	power spectral density predicted by Amiet's model
$S_{pp,\text{exact}}$	=	power spectral density predicted by exact model
S_{qq}	=	wave number cross spectrum of surface pressure
t	=	observer time
U_c	=	convection velocity
U_X	=	chordwise flow velocity
α	=	stagger angle
δ	=	boundary-layer thickness
Δr	=	span of blade section
κ	=	aeroacoustic coupling wave number
μ, μ_∞	=	acoustic reduced frequency without and with effects of skewed gusts
τ	=	retarded time
τ_w	=	wall shear stress
Φ_{pp}	=	surface pressure spectrum
Ω	=	rotor angular speed
ω	=	angular frequency
ω_ϕ, ω_k	=	Doppler-shifted angular frequency

Subscripts

Amiet	=	quantity related to Amiet's model
exact	=	quantity related to exact model
k	=	quantity depending on k
ϕ	=	quantity depending on ϕ

I. Introduction

THE prediction of the broadband noise from rotating blades is of interest in many industrial applications, such as aircraft propeller noise, helicopter noise, wind turbine noise, cooling fan noise, etc. Since the early 1970s, many empirical and semianalytical models have been developed to predict, and therefore reduce, both leading-edge and trailing-edge broadband noise from fans. The first general framework for broadband noise predictions from rotating blades is generally attributed to Ffowcs Williams and Hawkings [1], who applied the exact Ffowcs Williams and Hawkings (FWH) equation (see [2]) to point dipole sources in circular motion. This approach was first extended to noncompact acoustic sources in compressible flows by Homicz and George [3] for the case of broadband noise due to blade–turbulence interaction. Homicz and George related the unsteady blade loading to the turbulence spectrum using the compressible airfoil theory of Osborne [4]. Their formulation is quite general but was considered, at that time, as being very expensive computationally. Kim and George [5] were the first to use the exact FWH equation to develop a trailing-edge noise model for rotating blades, but they approximated the sound sources as a point dipoles.

To deal with the computational cost associated with the use of the FWH equation for rotating broadband noise sources, which was considered high at the time, Amiet [6] proposed a simplified alternative approach, which has been widely used since. This approach consists of approximating the noise from an airfoil in rotating motion by the average over the angular position of the noise from a translating airfoil. In other words, the circular motion is approximated by a series of translations over an infinitesimal distance, as shown in Fig. 1. Amiet stated in [6] that this approach is valid at high frequencies and low rotor speed, where the effects of rotation on the noise are weak. Amiet's method has been first applied to the leading-edge rotor noise by Paterson and Amiet [7] and to trailing-edge rotor noise by Schlinker and Amiet [8]. This formulation has been used extensively in recent years to predict the leading-edge and trailing-edge broadband noise of low-speed fans (see, for instance, Rozenberg et al. [9], Roger et al. [10], and Fedala et al. [11]), helicopter rotors (Amiet et al. [12,13]), wind turbines (Glegg et al. [14]), and open propellers (Pagano et al. [15]).

To the knowledge of the authors, there has been no published work on the validity of the approximations made in Amiet's model. In an attempt to better understand the range of validity of Amiet's model, it is proposed in the present work to compare it to an equivalent

Presented as Paper 2010-3797 at the 16th AIAA/CEAS Aeroacoustics Conference, Stockholm, Sweden, 7–9 June 2010; received 13 July 2010; accepted for publication 7 December 2010.

*Research Student, Fluid Dynamics and Acoustics Group, Institute of Sound and Vibration Research.

†Professor of Engineering Acoustics, Fluid Dynamics and Acoustics Group, Institute of Sound and Vibration Research.

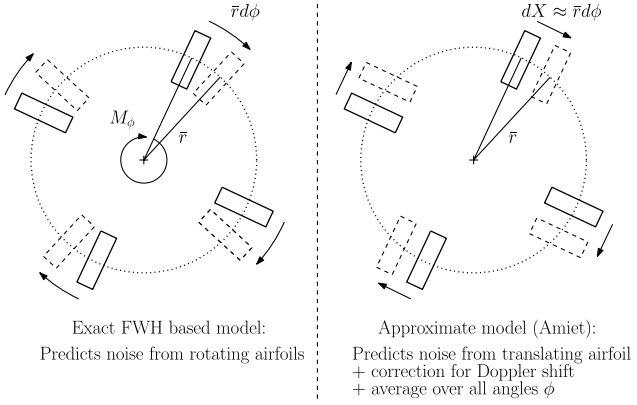

Fig. 1 Physical description of the exact model and the approximate Amiet's model [6].

FWH-based broadband noise model in which the effects of circular motion are treated exactly. The present study focuses on rotor trailing-edge noise only because, in the case of leading-edge noise, Amiet's formulation requires substantial modifications to capture the effects of blade-to-blade correlation due to turbulence ingestion (as explained in [13]).

The expressions used to predict the unsteady blade loading in the present study are very fast to compute; therefore, Amiet's model for deducing the noise of a rotating airfoil from the noise of a translating airfoil saves only little computational time compared with the exact FWH-based formulation. However, if more complex response models were used, such as a computational fluid dynamics (CFD)-based airfoil response function, for instance, Amiet's model would save significant computational time. This brings further motivation to understanding the general principles and limitations of Amiet's model for treating the effects of rotation on airfoil noise radiation.

In this paper, Amiet's model for rotor trailing-edge noise and an equivalent FWH-based model are first described in detail. The exact FWH-based model presented later in this paper is similar to the model due to Kim and George [5], except that the compact source approximation is relaxed. A comparative study is then presented between the FWH formulation and the approximate Amiet model. Criteria for the validity of Amiet's model are then proposed. Finally, according to these criteria, the validity of Amiet's model is tested for three practical applications: an open propeller, a model cooling fan, and a wind turbine.

II. Presentation of Models

In this section, the analytical formulations of Amiet's approximate model and the exact model are presented. Figure 2 describes the coordinate systems in which both models are expressed. The location of a far-field observer with respect to the center of a B-bladed rotor can be expressed in the spherical coordinate system (r_0, ψ_0, θ) or the Cartesian coordinate system (x, y, z). The location of the elemental force $d\mathbf{F}$, exerted by the blade on the fluid, can be expressed in the cylindrical coordinate system (r, ϕ, x) or in the airfoil-bound Cartesian coordinate system (r, X, Y), both centered at the midchord of the airfoil. The azimuthal Mach number of the elemental force $d\mathbf{F}$ is M_ϕ. The stagger angle is denoted by α, and an angle ψ is introduced to take into account the chordwise location of $d\mathbf{F}$. As in a wind tunnel, both the observer and the propeller are assumed to be stationary while a flow is passing through the rotor in the axial direction at Mach number M_x.

Sections II.A and II.B present the two propeller trailing-edge noise models under investigation and provide expressions for the power spectral density (PSD) S_{pp} of the acoustic pressure, radiated to the far field, in a form that facilitates their comparison. The narrowband sound pressure level (SPL), in decibels, is deduced from the expressions for S_{pp} as

$$\mathrm{SPL}\,(r_0, \theta, f) = 10\log_{10}\left(\frac{4S_{pp}(r_0, \theta, \omega)\Delta\omega}{(2.10^{-5})^2}\right) \tag{1}$$

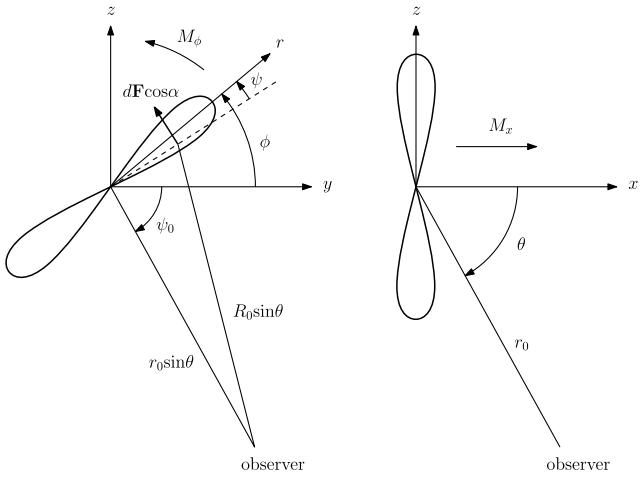

a) Propeller coordinates

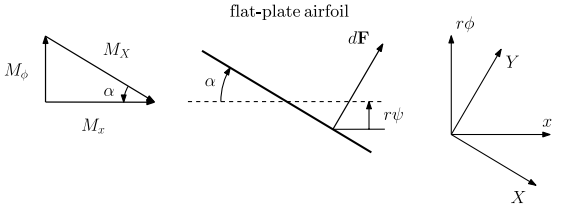

b) Airfoil-bound coordinates

Fig. 2 Coordinate systems defining the location of an elemental force $d\mathbf{F}$ on a propeller blade.

where the bandwidth is set equal to $\Delta\omega = 2\pi$ rad $\cdot$ s^{-1}, and where a factor of four is introduced, according to Moreau and Roger [16,17], in order to correct for the unsteady loading due to a turbulent flow passing the trailing edge of a flat plate. Neglecting the effects of mean flow convection, the sound power level (PWL), in decibels, is deduced from S_{pp} using

$$\mathrm{PWL}\,(f) = 10\log_{10}\left(\frac{4\Pi(\omega)\Delta\omega}{10^{-12}}\right) \tag{2}$$

where

$$\Pi(\omega) = \frac{2\pi r_0^2}{\rho_0 c_0}\int_0^\pi S_{pp}(r_0, \theta, \omega)\sin\theta\,\mathrm{d}\theta \tag{3}$$

In both Amiet's model and the exact model, strip theory is used in order to capture the spanwise variation of the aerodynamic parameters and the geometry. In the present paper, the two models are compared for a single strip of width Δr centered at a radius $\bar{r}$.

A. Amiet's Model for Propeller Trailing-Edge Noise

The starting point of Amiet's model is the observation from the work of Lowson [18] that the effect of rotation on noise generation is weak if the ratio of angular frequency over rotor speed is high (i.e., $\omega/\Omega \gg 1$). This has been confirmed by the work of Morfey and Tanna [19]. This condition of the validity of Amiet's model will be significantly revised in Sec. III.B.1 of this paper. Amiet's trailing-edge noise model for an isolated airfoil in translation (see [20]) can therefore be applied by considering a rotating motion as a series of translations over an infinitesimal distance. Furthermore, Amiet also introduces [6] the following corrections to take into account the main effects of rotation. The fact that a rotating blade segment is moving alternatively away from and toward the observer is taken into account by first substituting the angular frequency ω by a Doppler-shifted frequency ω_ϕ given by

$$\frac{\omega_\phi}{\omega} = 1 + M_\phi\cos\phi\sin\theta \tag{4}$$

where $M_\phi = \bar{r}\Omega/c_0$ is the rotation Mach number. Then, since the Doppler-shifted frequency ω_ϕ now varies with the azimuthal location $\phi = \Omega t$ of the airfoil, an averaging of the pressure spectrum over ϕ needs to be performed. With these corrections included, the PSD of the acoustic pressure radiated by B blades to the far field can be written as

$$S_{pp,\mathrm{Amiet}}(r_0, \psi_0, \theta, \omega) = \frac{B}{2\pi}\int_0^{2\pi}\left(\frac{\omega}{\omega_\phi}\right)^2 S_{pp,\phi}(r_0, \psi_0, \theta, \omega_\phi)\,\mathrm{d}\phi \quad (5)$$

The term $S_{pp,\phi}$ in Eq. (5) corresponds to the expression for the PSD of the trailing-edge noise due to a translating rectangular blade segment centered at a radius $\bar{r}$. It can be expressed in the airfoil-bound coordinate system $[(r-\bar{r}), X, Y]$ from [20,21] as

$$S_{pp,\phi}(r_0, \psi_0, \theta, \omega_\phi) = \frac{1}{8\pi}\left(\frac{\omega_\phi c Y}{2c_0\sigma^2}\right)^2 \Delta r |\mathcal{L}(0, K_{X,\phi}, \kappa_\phi)|^2 S_{qq}(0, K_{X,\phi}) \quad (6)$$

where $\sigma^2 = X^2 + \beta_X^2[(r-\bar{r})^2 + Y^2]$, $\beta_X = \sqrt{1-M_X^2}$, and the effects of skewed gusts are neglected (i.e., $k_r = 0$) by making the large span approximation, although this is not an essential requirement for the validity of Eq. (5). The subscript ϕ denotes a quantity dependent on the azimuthal location ϕ of the blade segment. The chordwise turbulence wave number and the aeroacoustic coupling wave number are, respectively, given by

$$K_{X,\phi} = \frac{\omega_\phi}{U_c} \quad \text{and} \quad \kappa_\phi = \frac{k_0}{\beta_X^2}\left(M_X - \frac{X}{\sigma}\right) \quad (7)$$

Schlinker and Amiet [8] assume a priori that the broadband self noise radiated to the far field is independent of the observer azimuthal coordinate ψ_0, which is equivalent to assuming that the observer is located in the (x, z) plane (cf. Fig. 2). The relation between the airfoil-bound coordinates $[(r-\bar{r}), X, Y]$ and the polar observer coordinates (r_0, θ), which includes the effect of stagger angle α and azimuthal angle ϕ, can be obtained from

$$\begin{bmatrix} r-\bar{r} \\ X \\ Y \end{bmatrix} = \mathcal{M}_\alpha \mathcal{M}_\phi \begin{bmatrix} r_0\cos\theta \\ 0 \\ r_0\sin\theta \end{bmatrix} \quad (8)$$

where the rotation matrices $\mathcal{M}_\alpha$ and $\mathcal{M}_\phi$ are defined by

$$\mathcal{M}_\alpha = \begin{bmatrix} 1 & 0 & 0 \\ 0 & -\sin\alpha & \cos\alpha \\ 0 & \cos\alpha & \sin\alpha \end{bmatrix}, \quad \mathcal{M}_\phi = \begin{bmatrix} 0 & \cos\phi & \sin\phi \\ 0 & -\sin\phi & \cos\phi \\ 1 & 0 & 0 \end{bmatrix} \quad (9)$$

The effects of mean flow convection are neglected in this study by setting $\beta_X = 1$ and $\kappa_\phi = -k_0 X/\sigma$ in Eqs. (6) and (7). The final expression of the far-field PSD of the rotor trailing-edge noise, as predicted by Amiet's model, can therefore be obtained by substituting Eqs. (6–9) into Eq. (5) as

$$S_{pp,\mathrm{Amiet}}(r_0, \theta, \omega) = \frac{B}{8\pi}\left(\frac{k_0 c}{2r_0}\right)^2 \Delta r \frac{1}{2\pi}\int_0^{2\pi} D_\phi(\theta,\alpha)|\mathcal{L}(0, K_{X,\phi}, \kappa_\phi)|^2 S_{qq}(0, K_{X,\phi})\,\mathrm{d}\phi \quad (10)$$

where

$$K_{X,\phi} = \frac{\omega_\phi}{U_c} \quad \text{and} \quad \kappa_\phi = k_0(\sin\theta\sin\alpha\cos\phi - \cos\theta\cos\alpha) \quad (11)$$

The convection velocity U_c is related to the chordwise flow velocity by $U_c = 0.8U_X$ (according to Amiet [20]), and a directivity term D_ϕ is introduced in Eq. (10) as

$$D_\phi(\theta,\alpha) = (\cos\theta\sin\alpha + \sin\theta\cos\alpha\cos\phi)^2 \quad (12)$$

The unsteady loading term $\mathcal{L}(k_r, k_X, \kappa)$ in Eq. (10) was derived by Roger and Moreau [22], who extended the earlier work of Amiet [20,21] to take into account the effects of skewed gust to give

$$\mathcal{L}(k_r, k_X, \kappa) = \frac{e^{2i\Theta_2}}{i\Theta_2}\left\{e^{-2i\Theta_2}\sqrt{\frac{\Theta_1}{\Theta_1-\Theta_2}}\mathrm{erf}[\sqrt{2i(\Theta_1-\Theta_2)}] - \mathrm{erf}[\sqrt{2i\Theta_1}] + 1\right\} \quad (13)$$

where the following notation has been introduced for the sake of brevity:

$$\begin{cases} \Theta_1 = \frac{c}{2}k_X + \mu_\infty + \mu M_X \\ \Theta_2 = \frac{c}{2}(k_X + \kappa) \end{cases} \quad (14)$$

and where $\mu = k_X M_c c/2\beta_X^2$, $\mu_\infty = \sqrt{\mu^2 - (k_r c/2\beta_X)^2}$ for supercritical gusts (i.e., $k_X M_c/k_r\beta_X > 1$) and $\mu_\infty = \sqrt{(k_r c/2\beta_X)^2 - \mu^2}$ for subcritical gusts (i.e., $k_X M_c/k_r\beta_X < 1$). However, since the effects of skewed gusts and mean flow convection effects are neglected in this study, Eq. (13) is used by setting $k_r = 0$ and $\beta_X = 1$.

Note that in the expression of κ_ϕ [Eq. (11)], the acoustic wave number k_0 is a function of the observer frequency ω rather than the Doppler-shifted frequency ω_ϕ. To the knowledge of the authors, this point is not explicitly made in Amiet's original work (see, for instance, [13]) and this might lead the reader to use in error $k_0 = \omega_\phi/c_0$ instead of $k_0 = \omega/c_0$ in Eq. (11). The wave number κ_ϕ appears in the term $\mathcal{L}(k_r, k_X, \kappa)$ as a coupling term between the wave number of the turbulence $K_{X,\phi}$ and the acoustic wave number k_0 of the sound radiation, and only the former can be affected by a Doppler shift resulting from rotation.

The wave number spectral density of the incident gust amplitudes S_{qq}, introduced in Eq. (10), is defined by Roger and Moreau [22] as

$$S_{qq}(0, k_X) = \tfrac{1}{\pi} l_r(k_X U_c)\Phi_{pp}(k_X U_c) \quad (15)$$

where $\Phi_{pp}(\omega)$ is the surface pressure spectral density close to the trailing edge, and the spanwise correlation length is given by $l_r(\omega) = 1.6U_c/\omega$, according to Brooks and Hodgson [23]. In this study, the semiempirical model for Φ_{pp} due to Goody [24] is used for comparison of the two models, and it is given by

$$\frac{\Phi_{pp}(\omega)U_X}{\tau_w^2\delta} = \frac{3.0\bar{\omega}^2}{[\bar{\omega}^{0.75} + 0.5]^{3.7} + [1.1R_T^{-0.57}\bar{\omega}]^7} \quad (16)$$

where $\tau_w = 0.5\rho_0 U_X^2 C_f$ is the wall shear stress, C_f is the friction coefficient, δ is the boundary-layer thickness, $\bar{\omega} = \omega\delta/U_X$ is a Strouhal number, and R_T is the ratio of outer-to-inner timescales of the turbulence given by

$$R_T = (\delta/U_X)/(\nu/u_\tau^2) = (u_\tau\delta/\nu)\sqrt{C_f/2}$$

B. Exact Model for Propeller Trailing-Edge Noise

In this section, a rotor trailing-edge noise model is described that treats the effects of rotation exactly, unlike the model due to Amiet [6], presented in the last section. The exact model describes the acoustic pressure field radiated to the far field using the exact FWH equation [2] for rotating dipole sources as

$$p(r_0, \psi_0, \theta, t) = -\int_{S_2}\nabla\cdot\left[\frac{d\mathbf{F}(r, X, Y, \tau)}{4\pi R_0}\right]_t \mathrm{d}S(r, X, Y) \quad (17)$$

where dS is a surface element on the blade, and the square brackets denote a quantity expressed at retarded time. Since the effects of mean flow on the acoustic radiation are neglected, the relation between observer time t and source time τ can be written as

$$\tau = t - R_0/c_0 \tag{18}$$

where R_0 is the distance between the elemental force $d\mathbf{F}$ and the observer, as shown in Fig. 2. Assuming that the observer is in the far field, the distance R_0 can be approximated in the amplitude terms by the distance r_0 between the center of the propeller disk and the observer. Further accuracy is required in the phase terms in order to capture the effects of rotation. The following first-order Taylor decomposition of R_0, obtained after some manipulation of the coordinate systems, is therefore used in the phase terms,

$$R_0 \approx r_0 - X\cos\alpha\cos\theta - r\sin\theta\cos(\phi - \psi + \psi_0) \tag{19}$$

The pressure jump $\Delta p = \|d\mathbf{F}\|$ due to the interaction between the turbulent boundary layer and the trailing edge of each blade is assumed to be incoherent from blade to blade. The noise due to a single blade is, therefore, predicted, and a factor B is introduced in the final expression for the PSD to account for the contribution of each blade. Because of the rotation of the blades, Δp is considered as a series of pulses repeating identically at every rotation of a blade and can be expressed as

$$\Delta p(r, X, \phi, \tau) = \Delta p(r, X, \tau) \sum_{k=-\infty}^{\infty} \delta(\phi - \Omega\tau - 2\pi k) \tag{20}$$

Following an approach similar to that of Blandeau and Joseph [25] for the broadband noise due to rotor-wake/rotor interaction in contrarotating open rotors, and considering only the $k_r = 0$ case (as in Sec. II.A), the PSD of the acoustic pressure radiated in the far field is given by

$$S_{pp,\text{exact}}(r_0, \theta, \omega) = \frac{B}{8\pi}\left(\frac{k_0 c}{2r_0}\right)^2 \Delta r \sum_{k=-\infty}^{\infty} D_k(\theta, \alpha, \omega)|\mathcal{L}(0, K_{X,k}, \kappa_k)|^2 S_{qq}(0, K_{X,k}) \tag{21}$$

where

$$K_{X,k} = \frac{\omega_k}{U_c} \quad \text{and} \quad \kappa_k = \frac{k}{r}\sin\alpha - k_0\cos\alpha\cos\theta \tag{22}$$

and a Doppler shift similar to that in Amiet's model [see Eq. (4)] has been defined by

$$\frac{\omega_k}{\omega} = 1 + k\frac{\Omega}{\omega} \tag{23}$$

The index k is the azimuthal acoustic mode order, and D_k is a directivity term defined as

$$D_k(\theta, \alpha, \omega) = \frac{1}{\Delta r}\int_{\bar{r}-(\Delta r/2)}^{\bar{r}+(\Delta r/2)} \left(\cos\theta\sin\alpha + \frac{k}{k_0 r}\cos\alpha\right)^2 J_k^2(k_0 r\sin\theta)\,\mathrm{d}r \tag{24}$$

The unsteady loading term $\mathcal{L}$ and the surface pressure cross spectrum S_{qq}, in Eq. (21), are the same as those defined for Amiet's model in the previous section.

Note that the model used for the spanwise correlation length l_r is not defined at $\omega = 0$, and this may generate discontinuities in the noise spectrum in the exact model when ω corresponds to multiples of the rotor angular speed Ω. This problem is avoided here by assuming that $S_{qq}(0, 0) = 0$. Moreover, because of the infinite summation over k in Eq. (21), the wave number $K_{X,k}$ can now take negative values. To prevent nonphysical discontinuities, the factor $1/\Theta_2 = 1/(\frac{c}{2}k_X + \frac{c}{2}\kappa)$ at the front of Eq. (13) must be replaced by $1/\Theta_2 = 1/(\frac{c}{2}|k_X| + \frac{c}{2}|\kappa|)$.

III. Comparative Study

A. Equivalence of Directivity Functions D in Both Models

Amiet's simplified model and the FWH-based model, in which the effects of rotation are treated exactly, have been expressed in the previous sections in a form that facilitates their comparison. It appears from Eqs. (10) and (21) that the two models can be expressed in fairly similar forms. However, three fundamental differences can be identified and are listed next:

1) The directivity terms in the two models [D_k and D_ϕ; see Eqs. (12) and (24), respectively] differ. The exact model includes a Bessel function of the first kind and an integral over the strip span, which are not appearing in Amiet's model.

2) The exact model presents an infinite sum over the azimuthal acoustic mode orders l, whereas Amiet's model involves an integral over the blade azimuth ϕ.

3) The expressions of the turbulent chordwise wave number K_X and the aeroacoustic coupling wave number κ are different in each model [see Eqs. (11) and (22)].

As a first step, both models are compared in terms of their directivity functions only. For this purpose, the preceding third point is neglected, and the source terms $|\mathcal{L}|^2$ and S_{qq} can therefore be taken outside of the integral and the summation in Eqs. (10) and (21), respectively. In this case, the only difference between the final expressions of the two models lies in the directivity functions,

$$D_{\text{exact}} = \sum_{k=-\infty}^{\infty} D_k$$

and

$$D_{\text{Amiet}} = \frac{1}{2\pi}\int_0^{2\pi} D_\phi\,\mathrm{d}\phi$$

of the exact model and of Amiet's model, respectively.

The directivity function D_{Amiet} of Amiet's model is obtained from Eq. (10) as

$$D_{\text{Amiet}} = \frac{1}{2\pi}\int_0^{2\pi} D_\phi(\theta, \alpha)\,\mathrm{d}\phi = \cos^2\theta\sin^2\alpha + \frac{1}{2}\sin^2\theta\cos^2\alpha \tag{25}$$

whereas the directivity function D_{exact} of the exact model is deduced directly from Eqs. (21) and (24) as

$$D_{\text{exact}} = \sum_{k=-\infty}^{\infty} D_l(\theta, \alpha, \omega) = \frac{1}{\Delta r}\sum_{k=-\infty}^{\infty}\int_{\bar{r}-(\Delta r/2)}^{\bar{r}+(\Delta r/2)} \left(\cos\theta\sin\alpha + \frac{k}{k_0 r}\cos\alpha\right)^2 J_k^2(k_0 r\sin\theta)\,\mathrm{d}r \tag{26}$$

The directivity function D_{exact} can alternatively be written by developing the parentheses in Eq. (26) as

$$D_{\text{exact}} = \frac{1}{\Delta r}\int_{\bar{r}-(\Delta r/2)}^{\bar{r}+(\Delta r/2)} (D_1 + D_2 + D_3)\,\mathrm{d}r \tag{27}$$

where

$$D_1 = (\cos\theta\sin\alpha)^2 \sum_{k=-\infty}^{\infty} J_k^2(k_0 r\sin\theta) \tag{28}$$

$$D_2 = \frac{2}{k_0 r}\cos\theta\cos\alpha\sin\alpha \sum_{k=-\infty}^{\infty} k J_k^2(k_0 r\sin\theta) \tag{29}$$

$$D_3 = \left(\frac{\cos\alpha}{k_0 r}\right)^2 \sum_{k=-\infty}^{\infty} k^2 J_k^2(k_0 r\sin\theta) \tag{30}$$

It can be shown that the infinite summations of Eqs. (28–30) converge, for any real argument ζ, to (cf. Appendix for mathematical proof)

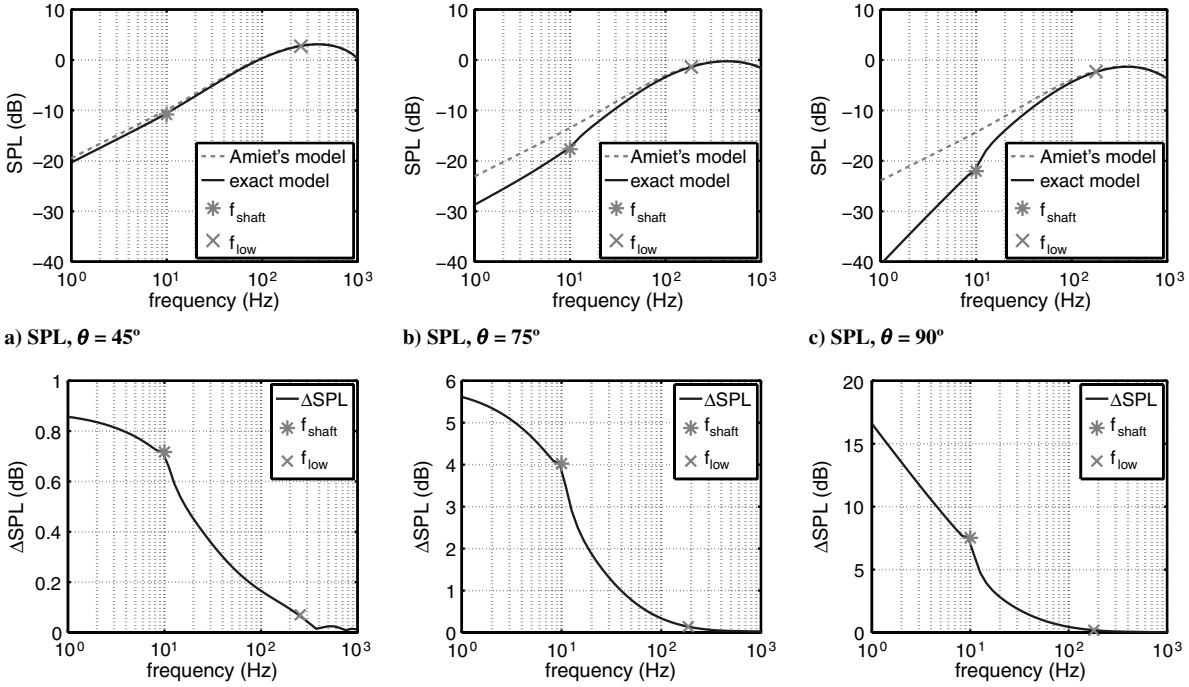

a) SPL, $\theta = 45°$ b) SPL, $\theta = 75°$ c) SPL, $\theta = 90°$

d) ΔSPL, $\theta = 45°$ e) ΔSPL, $\theta = 75°$ f) ΔSPL, $\theta = 90°$

Fig. 3 SPL predicted by Amiet's model and the exact model and $\Delta\mathrm{SPL} = 10\log_{10}(S_{pp,\mathrm{Amiet}}/S_{pp,\mathrm{exact}})$ for the observer angles $\theta = 45$, 75, and 90°.

$$\begin{cases} \sum_{k=-\infty}^{\infty} J_k^2(\zeta) = 1 \\ \sum_{k=-\infty}^{\infty} kJ_k^2(\zeta) = 0 \\ \sum_{k=-\infty}^{\infty} k^2 J_k^2(\zeta) = \frac{\zeta^2}{2} \end{cases} \tag{31}$$

Substituting Eq. (31) into Eqs. (28–30) and then into Eq. (27) therefore yields

$$D_{\mathrm{exact}} = \cos^2\theta\sin^2\alpha + \tfrac{1}{2}\sin^2\theta\cos^2\alpha = D_{\mathrm{Amiet}} \tag{32}$$

The preceding analysis shows that, in the case of equivalent source terms, the directivity functions of Amiet's model and the exact model are identical. This equivalence does not seem to have been recognized elsewhere and was unexpected, considering the fact that Amiet's model is not based on an exact acoustic formulation for rotating sources, whereas the exact model is. Moreover, Amiet developed [6] his model based on physical considerations and was unaware[‡] of the mathematical equivalence shown in the present section.

However, even though this result reinforces the confidence in the validity of Amiet's model, it does not prove equivalence between the two methods since the source terms $\mathcal{L}$ and S_{qq} in each model cannot be considered equivalent, as discussed later in Secs. III.B and III.C.

B. Comparison of Amiet's Model and Exact Model at Low Frequency

1. *Estimation of Low-Frequency Limit f_{low} of Validity of Amiet's Model*

As mentioned in Sec. II.A, Amiet [6] stated that his model should be valid at frequencies well above the shaft frequency of the rotor, so that the effects of rotation on the generation of sound can be neglected. Thus, over an acoustic period $2\pi/\omega$, the angular displacement of the blade can be neglected. In other words, Amiet gave an estimate of the low-frequency limit f_{low} of validity of his model as

$$f_{\mathrm{low}} \approx f_{\mathrm{shaft}} = \frac{\Omega}{2\pi} \tag{33}$$

A more accurate estimation of the low frequency f_{low} of the validity of Amiet's model is proposed in this section, based on the differences of the two models in predicting the directivity of the broadband noise at low frequencies.

It has been shown in Sec. III.A that the directivity functions of both models are equivalent if the expression for the source terms $|\mathcal{L}|^2$ and S_{qq} is assumed to be the same in both models. This assumption was made as a first step in the comparison of the two models but must be relaxed to allow a complete comparison.

From the properties of the function D_k [Eq. (24)], the exact model predicts that only the $k = 0$ azimuthal acoustic mode contributes to the radiated noise in the low-frequency limit. The second term in Eq. (24), which represents the contribution to the noise of the component of the unsteady blade loading in the torque direction (i.e., the azimuthal direction) must therefore vanish in the low-frequency limit. Thus, according to the exact model, the rotor trailing-edge broadband noise is controlled only by the component of the unsteady blade loading in the thrust direction (i.e., the axial direction) at frequencies where only the azimuthal acoustic mode of order $k = 0$ contributes to the radiated noise. This behavior cannot be captured by Amiet's model, since from Eq. (12), both the thrust and torque components of the unsteady blade loading contribute significantly to the noise in the low-frequency limit. Amiet's model must, therefore, differ from the exact model at frequencies lower than the cutoff frequency f_{low} of the first azimuthal mode of order $k = 1$, which is given by

$$f_{\mathrm{low}} = \frac{c_0}{2\pi\bar{r}\sin\theta} \tag{34}$$

This revised estimate of the low-frequency limit f_{low} of validity of Amiet's model is significantly different from Amiet's estimate, given in Eq. (34). Both conditions represent a critical frequency below which the effects of rotation can be considered important, but the effects of rotation are quantified differently, i.e., in terms of the rotor angular frequency Ω in Eq. (33) and in terms of the radial location $\bar{r}$ in Eq. (34). Moreover, unlike Eq. (33), the improved estimation of f_{low} presents a dependency on the observer angle. From Eq. (34), the low-frequency condition $f > f_{\mathrm{low}}$ of validity of Amiet's model can be alternatively rewritten as $2\pi\bar{r}\sin\theta > \lambda$ (where $\lambda = c_0/f$ is the acoustic wavelength). This physically means that Amiet's model must be valid for acoustic wavelengths smaller than the distance $2\pi\bar{r}$

[‡]Private communication with Roy K. Amiet, 25 May 2010.

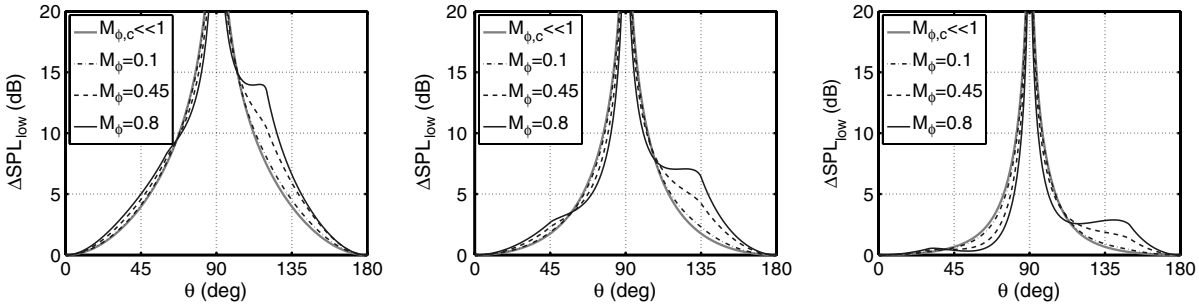

a) $\alpha = 30^o$ b) $\alpha = 45^o$ c) $\alpha = 60^o$

Fig. 4 Variation of $\Delta\mathrm{SPL}_{\mathrm{low}}$ with θ for a) $\alpha = 30°$, b) $\alpha = 45°$, c) $\alpha = 60°$, and $M_\phi = 0.1$, 0.45, and 0.8.

covered by the blade segment during one rotation, projected in the direction of the observer.

Figure 3 presents a comparison between SPLs (at 1 m) predicted by Amiet's model and the exact model for $\theta = 45$, 75, and 90°. The configuration used is a single spanwise strip of the model cooling fan described in Sec. IV.A. It appears from these plots that the expression of f_{low} introduced in this section [Eq. (34)] predicts more accurately the low-frequency limit of validity of Amiet's model than the condition $f_{\mathrm{low}} \approx f_{\mathrm{shaft}}$ [Eq. (33)], introduced by Amiet in [6]. Note that the ratio $\Delta\mathrm{SPL} = 10\log_{10}(S_{pp,\mathrm{Amiet}}/S_{pp,\mathrm{exact}})$ between the predictions of Amiet's model and the exact model tends in the low-frequency limit to a value independent of frequency, denoted here by

$$\Delta\mathrm{SPL}_{\mathrm{low}} = \lim_{f/f_{\mathrm{low}}\to 0} \Delta\mathrm{SPL}$$

except for the case $\theta = 90°$. An estimate for $\Delta\mathrm{SPL}_{\mathrm{low}}$ is given in the next section.

2. Estimation of Low-Frequency Error $\Delta\mathrm{SPL}_{\mathrm{low}}$ of Amiet's Model

An estimate for the error of Amiet's model $\Delta\mathrm{SPL}_{\mathrm{low}}$ in the low-frequency limit is now derived. Noting from Eq. (13) that

$$\lim_{f\to 0}\mathcal{L} = 1/\left(\frac{c}{2}|k_X| + \frac{c}{2}|\kappa|\right)$$

and that $\Phi_{pp}(\omega)$ is proportional to ω^2 in the low-frequency limit [from Eq. (16)]; an exact value of the low-frequency error of Amiet's model can be obtained from Eqs. (10) and (21) as

$$\lim_{f/f_{\mathrm{low}}\to 0} \frac{S_{pp,\mathrm{Amiet}}}{S_{pp,\mathrm{exact}}} = \frac{1}{2\pi}\int_0^{2\pi} \frac{(1 + M_c|\cos\theta\cos\alpha|)^2[1 + (\tan\theta/\tan\alpha)\cos\phi]^2(1 + M_\phi\sin\theta\cos\phi)}{(1 + M_\phi\sin\theta\cos\phi + M_c|\sin\alpha\sin\theta\cos\phi - \cos\theta\cos\alpha|)^2}\,\mathrm{d}\phi \tag{35}$$

The integral in Eq. (35) does not seem to have a simple analytical solution valid for all values of θ, α, M_ϕ, and M_c. However, a simple solution of Eq. (35) exists in the low Mach number limit (i.e., $(M_\phi, M_c) \ll 1$), which gives the following approximate expression for $\Delta\mathrm{SPL}_{\mathrm{low}}$ (in decibels):

$$\lim_{(M_\phi,M_c)\to 0} \Delta\mathrm{SPL}_{\mathrm{low}} = 10\log_{10}\left\{1 + \frac{1}{2}\left(\frac{\tan\theta}{\tan\alpha}\right)^2\right\} \tag{36}$$

Figure 4 shows the variation of the exact [Eq. (35)] and low Mach number [Eq. (36)] estimates of $\Delta\mathrm{SPL}_{\mathrm{low}}$ as a function of the observer angle θ and for $M_\phi = 0.1$, 0.45, and 0.8, and $\alpha = 30$, 45, and 60°. For any configuration, $\Delta\mathrm{SPL}_{\mathrm{low}}$ is zero for an observer on the rotor axis ($\theta = 0°$ and $\theta = 180°$) and tends to infinity for an observer located in the rotor plane ($\theta = 90°$). This result can be explained by noting, from Sec. III.B.1, that $\Delta\mathrm{SPL}_{\mathrm{low}}$ must be large if the component of the unsteady blade loading in the torque direction is large compared with the component in the thrust direction. However, according to Eqs. (12) and (24), the thrust component vanishes when the observer is in the rotor plane ($\theta = 90°$), whereas the torque component vanishes when the observer is on the rotor axis ($\theta = 0°$ and $\theta = 180°$), thus explaining the shape of $\Delta\mathrm{SPL}_{\mathrm{low}}$ shown in Fig. 4. Note also that $\Delta\mathrm{SPL}_{\mathrm{low}}$ is weakly affected by changes in M_ϕ and is higher for small stagger angles α for any given observer angle $\theta \neq 90°$. These results confirm the behavior observed in Fig. 3.

C. Comparison of Amiet's Model and Exact Model at High Frequency

1. Estimation of High-Frequency Limit f_{high} of Validity of Amiet's Model

In both models under investigation, the streamwise turbulence wave number k_X is Doppler-shifted in order to capture the effects of source rotation [see Eqs. (4), (11), (22), and (23)]. The expressions for those Doppler shifts are different in both models, but the range of shifted frequencies as ϕ varies is approximately the same. Thus, the maximum value of the Doppler shift for Amiet's model is obtained for $\phi = 0$, whereas the maximum value of the Doppler shift for the exact model is obtained for $k_{\max} \approx k_0\bar{r}\sin\theta$ (from the property of Bessel functions of the first kind), which yields from Eqs. (4) and (23)

$$\left.\frac{\omega_k}{\omega}\right|_{\max} = 1 + k_{\max}\Omega/\omega \approx 1 + M_\phi\sin\theta = \left.\frac{\omega_\phi}{\omega}\right|_{\max} \tag{37}$$

Since the range of shifted frequencies is not exactly the same, a small error exists between the two models, and this error must become significant in regions where the boundary-layer pressure spectrum scales with k_X to a high power. This typically occurs in the high-frequency limit, where the surface pressure spectrum Φ_{pp} scales with k_X^{-5} [see Eq. (16)]. It is therefore proposed to associate the critical frequency f_{high} with the turning point where Φ_{pp} enters its high-frequency asymptotic region. Assuming that this turning point is accurately predicted by the model for Φ_{pp} proposed by Goody [24], an estimate for f_{high} can be identified from Eq. (16) as the frequency above which the second term in the denominator becomes dominant compared with the first term:

$$f_{\mathrm{high}} \approx 3.0\,\frac{U_X R_T^{0.57}}{2\pi\delta} \tag{38}$$

where R_T is introduced in Eq. (16) and deduced from the turbulent boundary layer on the suction side of the airfoil, and where the factor 3.0 has been set empirically.

Figure 5 presents a validation of Eq. (38) by plotting the difference in SPL, $\Delta\mathrm{SPL} = \mathrm{SPL}_{\mathrm{Amiet}} - \mathrm{SPL}_{\mathrm{exact}}$, predicted by each model. The rotation Mach number M_ϕ is kept constant while ΔSPL is estimated at several stagger angles α; therefore, several values of f_{high} (since

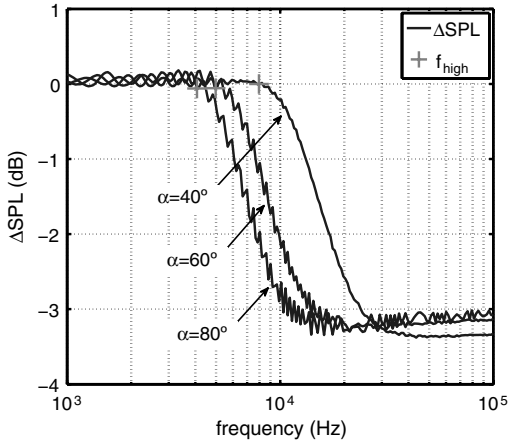

Fig. 5 Validation of f_{high} for $\alpha = 40$, 60, and 80°; $M_\phi = 0.6$ and $\theta = 90°$.

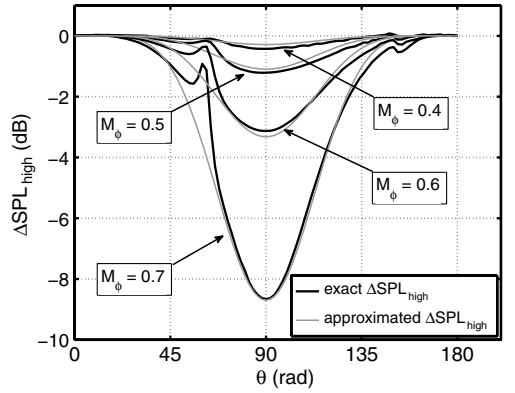

Fig. 6 Variation of the high-frequency error $\Delta\text{SPL}_{\text{high}}$ of Amiet's model with M_ϕ and θ.

$U_X = M_\phi c_0/\sin\alpha$) are evaluated. The observer angle is set to $\theta = 90°$, so that the effects of the Doppler shifts are maximum. The baseline configuration chosen here consists of a single blade segment ($B = 1$) of chord $c = 0.4$ m, span $\Delta r = 0.6$ m, and stagger angle $\alpha = 60°$, rotating at $M_\phi = 0.6$ and located radially at $\bar{r} = 1$ m from the center of rotation. The main turbulent boundary-layer parameters required in the surface pressure spectrum used here [Eq. (17)] are the boundary-layer thickness and the friction coefficient, set to $\delta = 5$ cm and $C_f = 10^{-5}$, respectively. This configuration has been chosen arbitrarily, without any loss of generality, so that the high-frequency error of Amiet's model appears clearly in Fig. 5. Practical applications to realistic rotor configurations are presented in Sec. IV.A.

Table 1 Main parameters used for the applications considered

	Model cooling fan	Open propeller	Wind turbine
R_t, m	0.4	1.8 (typical)	29
α, °	56	73 (takeoff), 52 (cruise)	80
c, m	0.13	0.31 (estimated)	2 (estimated)
B	2	6	3
Ω, rad · s^{-1}	62.83	188.5	2.618
M_ϕ	0.0525	0.748	0.165

The estimate for f_{high} given in Eq. (38) accurately predicts the high-frequency limit at which Amiet's model starts to deviate from the exact model, in Fig. 5. Note also in Fig. 5 that ΔSPL converges to a value, denoted here by $\Delta\text{SPL}_{\text{high}}$, that is independent of frequency and weakly dependent on stagger angle. An estimate for $\Delta\text{SPL}_{\text{high}}$ is given in the next section.

2. *Estimation of High-Frequency Error $\Delta\text{SPL}_{\text{high}}$ of Amiet's Model*

Because of the complexity of Eqs. (10) and (21), it is difficult to establish an exact analytical expression for the high-frequency error $\Delta\text{SPL}_{\text{high}}$ between Amiet's model and the exact model. However, it has been observed that $\Delta\text{SPL}_{\text{high}}$ varies mostly as a function of $M_\phi \sin\theta$, which corresponds to the main term of the Doppler shifts responsible for the high-frequency error of Amiet's model [see Eq. (37)]. Figure 6 presents plots of $\Delta\text{SPL}_{\text{high}}$ as a function of θ for different values of M_ϕ, for the configuration described in Sec. III.C.1. These plots were obtained at the unrealistically high frequency of $f = 100$ kHz, where $\Delta\text{SPL}_{\text{high}}$ has converged to a value independent of frequency (as shown in Fig. 5). An empirical estimate of $\Delta\text{SPL}_{\text{high}}$ is obtained by curve fitting the exact value to give

$$\Delta\text{SPL}_{\text{high}} \approx A\log_{10}\{1 - (M_\phi \sin\theta)^6\} \tag{39}$$

where A is an arbitrary constant set equal to $A = 160$.

Reasonable agreement is shown in Fig. 6 between the approximated $\Delta\text{SPL}_{\text{high}}$ of Eq. (39) and the exact value of $\Delta\text{SPL}_{\text{high}}$. Equation (39) can therefore be used as an estimate of the high-frequency error between Amiet's model and the exact model, when the frequency is above the high-frequency limit of validity f_{high}, given in Eq. (38).

IV. Applications and Discussion of Domain of Validity of Amiet's Model

A. Applications

The results presented in Sec. III show that Amiet's model and the exact model for propeller trailing-edge noise agree better than 0.1 dB over a frequency range bounded by the frequencies f_{low} and f_{high} [Eqs. (34) and (38)]. Approximate estimates of the low- and high-frequency error $\Delta\text{SPL}_{\text{low}}$ and $\Delta\text{SPL}_{\text{high}}$ of Amiet's model, beyond these critical frequencies, have also been proposed in this paper [Eqs. (36) and (39)].

The criteria defining the validity of Amiet's model are now applied to different realistic industrial fans and rotors. Three different applications are chosen on the basis that they all have been the subject of published studies of trailing-edge noise. They consist of an open propeller [15,26] (at takeoff and cruise conditions), a model cooling fan [9], and a wind turbine [27]. Note that the trailing-edge noise model due to Amiet [6], assessed in this paper, was in fact used in these references to predict the broadband noise of the open propeller [15,26] and the model cooling fan [9], whereas the semiempirical method of Brooks et al. [28] was used for predicting the broadband noise from the wind turbine [27].

In this section, Amiet's model and the exact model are compared, for all rotor configurations, by predicting the trailing-edge noise directivity and PWL spectrum of a representative blade section located at three-quarters of the tip radius (i.e., $\bar{r} = 0.75R_t$). The span of the blade section considered is set to be equal to a third of its radial

Table 2 Estimates of the validity of Amiet's model applied to the four configurations considered

	f_{shaft}, Hz	f_{low} ($\theta = 90°$), Hz	$\Delta\text{SPL}_{\text{low}}$ ($\theta = 60°$), dB	f_{high}, Hz	$\Delta\text{SPL}_{\text{high}}$ ($\theta = 90°$), dB
Model cooling fan	10	180	1	500	≈ 0
Open propeller at cruise	30	40	3	2.3×10^5	-13
Open propeller at takeoff	30	40	1	1.7×10^5	-13
Wind turbine	0.42	2.5	<1	6520	≈ 0

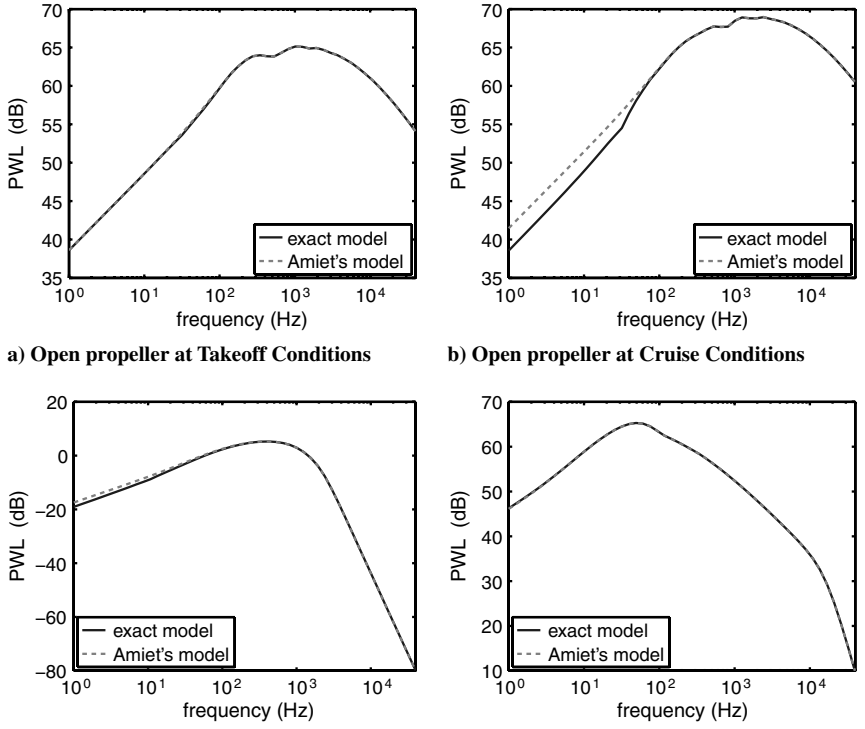

a) Open propeller at Takeoff Conditions

b) Open propeller at Cruise Conditions

c) Model cooling fan

d) Wind turbine

Fig. 7 PWL predictions, using Amiet's model and the exact model, of the trailing-edge noise due to a single strip of an open propeller at a) takeoff and b) cruise conditions; c) a model cooling fan and d) a wind turbine.

location (i.e., $\Delta r = \bar{r}/3$). The panel method software XFOIL is used to obtain the boundary-layer parameters required for the trailing-edge broadband noise models. Since no blade geometry is provided in the references (except for the cooling fan in [9]), and since the interest is in comparing the trailing-edge noise models, rather than producing highly accurate noise predictions, a NACA0012 airfoil geometry is used as input into the XFOIL code for all the rotor configurations. It is also assumed, without loss of generality, that the angle of attack is zero in all configurations.

The main geometry and aerodynamic parameters used in this study are given in Table 1. The tip radius of the open propeller is not provided in [15,26] and is therefore set arbitrarily to $R_t = 1.8$ m, which is a typical value for open propellers. Note that the stagger angle α is the only parameter modified between the takeoff and the cruise conditions for the open propeller configuration. An approximate value of the chord of the open propeller and the wind turbine, at 75% of R_t, has been deduced graphically from the sketches provided in [15,26,27].

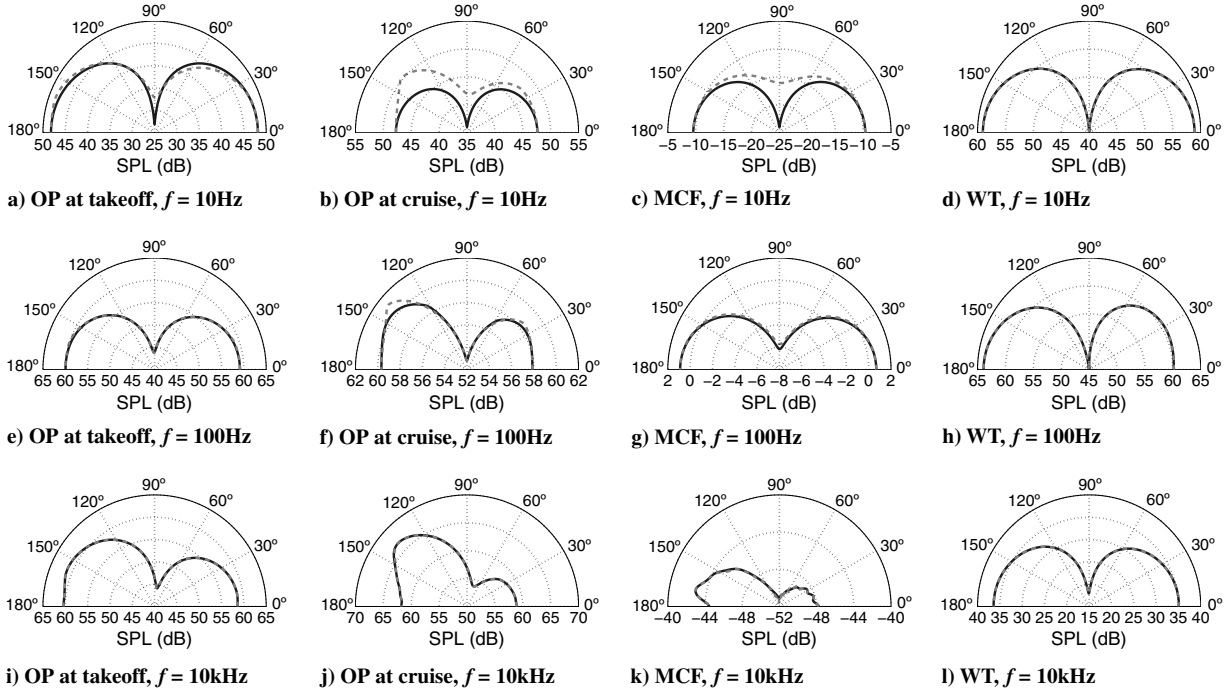

a) OP at takeoff, f = 10Hz

b) OP at cruise, f = 10Hz

c) MCF, f = 10Hz

d) WT, f = 10Hz

e) OP at takeoff, f = 100Hz

f) OP at cruise, f = 100Hz

g) MCF, f = 100Hz

h) WT, f = 100Hz

i) OP at takeoff, f = 10kHz

j) OP at cruise, f = 10kHz

k) MCF, f = 10kHz

l) WT, f = 10kHz

Fig. 8 Directivity of SPL (at 1 m) at a–d) $f = 10$ Hz, e–h) $f = 100$ Hz, and i–l) $f = 10$ kHz for the open propeller (OP) at takeoff and cruise, the model cooling fan (MCF), and the wind turbine (WT). Amiet's model: dashed line; exact model: solid line.

The main criteria for the validity of Amiet's model, introduced in Sec. III, are applied to the three cases considered and are summarized in Table 2. The maximum values of f_{low} and $\Delta\text{SPL}_{\text{high}}$ (i.e., at $\theta = 90°$) are shown, and an estimate of $\Delta\text{SPL}_{\text{low}}$ is given at $\theta = 60°$ using Eq. (36). Figure 7 presents predictions of PWL using both the exact model and Amiet's model for the four configurations considered. Agreement better than 0.5 dB is generally observed between the two models for frequencies above f_{low}. The low-frequency error $\Delta\text{SPL}_{\text{low}}$ and the low-frequency limit f_{low} of Amiet's model agree well with the values predicted in Table 2. Moreover, the high-frequency error $\Delta\text{SPL}_{\text{high}}$ of Amiet's model is either negligible (for the cooling fan and the wind turbine) or significant (for the open propeller) but only at frequencies $f > f_{\text{high}}$ well above the audible frequency range, as shown in Table 2.

Figure 8 presents directivity patterns predicted by both methods for the four rotor configurations considered at $f = 10$ Hz, $f = 100$ Hz, and $f = 10$ kHz. In these directivity plots, Amiet's model and the exact model differ only at very low frequencies ($f = 10$ Hz), as already observed for PWL in Fig. 7. At frequencies $f = 100$ Hz and $f = 10$ kHz, which are within the audible range, the agreement of these directivity plots is excellent, and the difference in SPL between the two models is within 1 dB.

B. Discussion of Validity of Amiet's Model

Despite the important theoretical differences presented in Sec. III, the approximations made in Amiet's model for the noise due to a rotating blade section seem to impact very little on the noise predictions over the audible frequency range. For the configurations studied, both models provide predictions of PWL and directivity that differ by less than 0.5 and 1 dB, respectively. It has been shown that the error of Amiet's model can become significant, but the frequencies at which this occurs are generally either too low or too high to be of significance in evaluating subjective indicators of noise, such as effective perceived noise-level. Thus, this paper formally establishes the validity of Amiet's assumption [6] that, over most of the audible frequency range, the effects of rotation on rotor broadband noise can be included by means of averaging over the angular position of a locally translating airfoil, as shown in Fig. 1.

As mentioned in Sec. I, the difference in computational time between the two models compared in this study is not significant, since the analytical isolated flat-plate response functions used in this paper [Eq. (13)] are fast to compute. However, Amiet's approach for deducing the noise of rotating airfoil from translating airfoil noise models may save significant computational time if more complex models are used for the blades response function. The very good agreement observed in this study between the approximate model and the exact model indicate that applications of Amiet's model to response models such as, for instance, CFD-based models that can take into account realistic airfoil geometries (see, for instance, Sandberg and Sandham [29]) may be feasible and should be investigated in subsequent work.

V. Conclusions

In conclusion, the approximate model due to Amiet [6] for predicting the trailing-edge noise from rotating blade sections has been compared with an exact model based on the FWH equation for rotating sources of sound. The two models have been analytically expressed in a form that facilitates their comparison, and equivalence of their directivity functions has been shown. Amiet's model exhibits excellent agreement with the exact model over the midfrequency range but diverges in the low- and high-frequency limits. Conditions for the low- and high-frequency limits of the validity of Amiet's model have been established. Estimates of the error of Amiet's model in the low- and high-frequency limits have been provided. The two trailing-edge noise models have been applied to practical applications, including an open aircraft propeller, a model cooling fan, and a wind turbine. It has been shown that the domain of validity of Amiet's model covers most of the domain of frequencies of interest for the configurations studied.

Appendix: Mathematical Proof of Equivalence of D_{Amiet} and D_{exact}

In this Appendix, the mathematical proofs of the identities of Eq. (31) are presented. All these identities are particular cases of known theorems that can be found, for instance, in Abramowitz and Stegun [30].

The first identity of Eq. (31) can be proved from Neumann's addition theorem for Bessel functions of the first kind (from Eq. 9.1.75 in [30]), which states that

$$\sum_{k=-\infty}^{\infty} J_{\nu\mp k}(u)J_k(v) = J_\nu(u \pm v) \tag{A1}$$

for any integer ν and any reals u and v. Setting $u = v = \zeta$ and $\nu = 0$ in Eq. (A1) and noting that $J_0(0) = 1$ yields

$$\sum_{k=-\infty}^{\infty} J_k^2(\zeta) = 1 \tag{A2}$$

The second identity comes from the property of Bessel functions of the first kind, stating that $J_{-k}^2(\zeta) = J_k^2(\zeta)$. For any real argument ζ, the following identity can then be proved by recurrence that

$$\sum_{k=-\infty}^{\infty} kJ_k^2(\zeta) = 0 \tag{A3}$$

The third identity can be proved from Gegenbauer's addition theorem for Bessel functions of the first kind (Eq. 9.1.80 in [30]), which states that

$$2^\nu\Gamma(\nu)\sum_{k=0}^{\infty}(\nu+k)\frac{J_{\nu+k}(u)}{u^\nu}\frac{J_{\nu+k}(v)}{v^\nu}C_k^{(\nu)}(\cos\alpha) = \frac{J_\nu(w)}{w^\nu} \tag{A4}$$

where ν is any positive, nonzero integer, u and v are any reals, $w = \sqrt{u^2 + v^2 - 2uv\cos\alpha}$, and $C_k^{(\nu)}(z)$ is Gegenbauer's polynomial. Setting $\nu = 1$, $u = v = \zeta$, and $\alpha = 0$, and using the fact that $C_k^1(1) = 1 + k$ and

$$\lim_{w\to 0} J_1(w)/w = 1/2$$

yields

$$2\sum_{k=0}^{\infty}(k+1)^2J_{k+1}^2(z) = \frac{\zeta^2}{2} \tag{A5}$$

which can be extended to negative k values as

$$\sum_{k=-\infty}^{\infty} k^2J_k^2(\zeta) = \frac{\zeta^2}{2} \tag{A6}$$

Acknowledgments

The research leading to these results has received funding from the European Community's Seventh Framework Programme FP7/2007-2013 under grant agreement 211861, Validation of Radical Engine Architecture Systems, and from Rolls–Royce, plc. The authors would also like to thank Roy Amiet for his explanations regarding the approximate model and for his valuable comments of the results of this paper.

References

[1] Ffowcs Williams, J. E., and Hawkings, D. L., "Theory Relating to the Noise of Rotating Machinery," *Journal of Sound and Vibration*, Vol. 10, No. 1, 1969, pp. 10–21. doi:10.1016/0022-460X(69)90125-4

[2] Ffowcs Williams, J. E., and Hawkings, D. L., "Sound Generation by Turbulence and Surfaces in Arbitrary Motion," *Philosophical Transactions of the Royal Society of London. Series A, Mathematical and Physical Sciences*, Vol. 264, No. 1151, 1969, pp. 321–342.

doi:10.1098/rsta.1969.0031
[3] Homicz, G., and George, A., "Broadband and Discrete Frequency Radiation from Subsonic Rotors," *Journal of Sound and Vibration*, Vol. 36, No. 2, 1974, pp. 151–177. doi:10.1016/S0022-460X(74)80292-0
[4] Osborne, C., "Unsteady Thin-Airfoil Theory for Subsonic Flow," *AIAA Journal*, Vol. 11, No. 2, 1973, pp. 205–209. doi:10.2514/3.6730
[5] Kim, Y. N., and George, A. R., "Trailing-Edge Noise from Hovering Rotors," *AIAA Journal*, Vol. 20, No. 9, 1982, pp. 1167–1174. doi:10.2514/3.51176
[6] Amiet, R. K., "Noise Produced by Turbulent Flow into a Propeller or Helicopter Rotor," *AIAA Journal*, Vol. 15, No. 3, 1977, pp. 307–308. doi:10.2514/3.63237
[7] Paterson, R. W., and Amiet, R. K., "Noise of a Model Helicopter Rotor due to Ingestion of Turbulence," NASA, TR 3213, 1979.
[8] Schlinker, R. H., and Amiet, R. K., "Helicopter Rotor Trailing Edge Noise," NASA, TR 3470, 1981.
[9] Rozenberg, Y., Roger, M., and Moreau, S., "Rotating Blade Trailing-Edge Noise: Experimental Validation of Analytical Model," *AIAA Journal*, Vol. 48, No. 5, 2010, pp. 951–962. doi:10.2514/1.43840
[10] Roger, M., Moreau, S., and Guedel, A., "Broadband Fan Noise Prediction Using Single-Airfoil Theory," *Noise Control Engineering Journal*, Vol. 54, No. 1, 2006,pp. 5–14. doi:10.3397/1.2888773
[11] Fedala, D., Kouidri, S., Rey, R., Carolus, T., and Schneider, M., "Incident Turbulence Interaction Noise from an Axial Fan," 12th AIAA/CEAS Aeroacoustics Conference, Cambridge, MA, AIAA Paper 2006-2477, 2006.
[12] Amiet, R. K., Simonich, J. C., and Schlinker, R. H., "Rotor Noise due to Atmospheric Turbulence Ingestion. Part II: Aeroacoustic Results," *Journal of Aircraft*, Vol. 27, No. 1, 1990, pp. 15–22. doi:10.2514/3.45892
[13] Amiet, R. K., "Noise Produced by Turbulent Flow Into Rotor: Theory Manual for Noise Calculation," NASA, TR 181788, 1989.
[14] Glegg, S. A. L., Baxter, S. M., and Glendinning, A. G., "The Prediction of Broadband Noise from Wind Turbines," *Journal of Sound and Vibration*, Vol. 118, No. 2, 1987, pp. 217–239. doi:10.1016/0022-460X(87)90522-0
[15] Pagano, A., Barbarino, M., Casalino, D., and Federico, L., "Tonal and Broadband Noise Calculations for Aeroacoustic Optimization of Pusher Propeller," *Journal of Aircraft*, Vol. 47, No. 3, 2010, pp. 835–848. doi:10.2514/1.45315
[16] Moreau, S., and Roger, M., "Back-Scattering Correction and Further Extensions of Amiet's Trailing-Edge Noise Model. Part II: Application," *Journal of Sound and Vibration*, Vol. 323, Nos. 1–2, 2009, pp. 397–425. doi:10.1016/j.jsv.2008.11.051
[17] Roger, M., and Moreau, S., "Extension and Limitations of Analytical Airfoils Broadband Noise Models," *International Journal of Aeroacoustics*, Vol. 9, No. 3, 2010, pp. 273–305. doi:10.1260/1475-472X.9.3.273
[18] Lowson, M. V., "The Sound Field for Singularities in Motion," *Proceedings of the Royal Society of London. Series A, Mathematical and Physical Sciences*, Vol. 286, No. 1407, 1965, pp. 559–572. doi:10.1098/rspa.1965.0164
[19] Morfey, C. L., and Tanna, H. K., "Sound Radiation from a Point Force in Circular Motion," *Journal of Sound and Vibration*, Vol. 15, No. 3, 1971, pp. 325–351. doi:10.1016/0022-460X(71)90428-7
[20] Amiet, R. K., "Noise due to Turbulent Flow Past a Trailing Edge," *Journal of Sound and Vibration*, Vol. 47, No. 3, 1976, pp. 387–393. doi:10.1016/0022-460X(76)90948-2
[21] Amiet, R. K., "Effect of the Incident Surface Pressure Field on Noise due to Turbulent Flow Past a Trailing Edge," *Journal of Sound and Vibration*, Vol. 57, No. 2, 1978, pp. 305–306. doi:10.1016/0022-460X(78)90588-6
[22] Roger, M., and Moreau, S., "Back-Scattering Correction and Further Extensions of Amiet's Trailing-Edge Noise Model. Part 1: Theory," *Journal of Sound and Vibration*, Vol. 286, No. 3, 2005, pp. 477–506. doi:10.1016/j.jsv.2004.10.054
[23] Brooks, T. F., and Hodgson, T. H., "Trailing Edge Noise Prediction from Measured Surface Pressures," *Journal of Sound and Vibration*, Vol. 78, No. 1, 1981, pp. 69–117. doi:10.1016/S0022-460X(81)80158-7
[24] Goody, M., "Empirical Spectral Model of Surface Pressure Fluctuations," *AIAA Journal*, Vol. 42, No. 9, 2004, pp. 1788–1794. doi:10.2514/1.9433
[25] Blandeau, V. P., and Joseph, P. F., "Broadband Noise due to Rotor-Wake/Rotor Interaction in Contra-Rotating Open Rotors," *AIAA Journal*, Vol. 48, No. 11, 2010, pp. 2674–2686. doi:10.2514/1.J050566
[26] Pagano, A., Federico, L., Barbarino, M., Guida, F., and Aversano, M., "Multi-Objective Aeroacoustic Optimization of an Aircraft Propeller," 12th AIAA/ISSMO Multidisciplinary Analysis and Optimization Conference, Victoria, B.C., Canada, AIAA Paper 2008-6059, 2008.
[27] Oerlemans, S., Sijtsma, P., and Mendez Lopez, B., "Location and Quantification of Noise Sources on a Wind Turbine," *Journal of Sound and Vibration*, Vol. 299, Nos. 4–5, 2007, pp. 869–883. doi:10.1016/j.jsv.2006.07.032
[28] Brooks, T. F., Pope, D. S., and Marcolini, M. A., "Airfoil Self-Noise and Prediction," NASA, TR1218, 1989.
[29] Sandberg, R. D., and Sandham, N. D., "Direct Numerical Simulation of Turbulent Flow Past a Trailing Edge and the Associated Noise Generation," *Journal of Fluid Mechanics*, Vol. 596, 2008, pp. 353–385. doi:10.1017/S0022112007009561
[30] Abramowitz, M., and Stegun, I., *Handbook of Mathematical Functions with Formulas, Graphs, and Mathematical Table*, Courier Dover Publications, New York, 1965, p. 363.

M. Glauser
Associate Editor